Tomographic MAX-DOAS observations of sun-illuminated targets: a new technique providing well-defined absorption paths in the boundary layer

Erna Frins[1], Nicole Bobrowski[2], Ulrich Platt[2], Thomas Wagner[2]

[1]Instituto de Física, Facultad de Ingeniería, J. Herrera y Reissig 565, Montevideo, Uruguay

[2]Institut für Umweltphysik, University of Heidelberg, Im Neuenheimer Feld 229, D-69120 Heidelberg, Germany

Abstract. A novel experimental procedure to measure the surface-near distribution of atmospheric trace gases using passive Multi-Axis-Differential Absorption Optical Spectroscopy (MAX-DOAS) is proposed. The idea consists of pointing the receiving telescope of the spectrometer to non-reflecting surfaces or to 'bright' targets placed at known distances from the measuring device, which are illuminated by sunlight. We show that the partial trace gas absorptions between the top of the atmosphere and the target can be easily removed from the measured total absorption. Thus it is possible to derive the average concentration of trace gases like e.g. NO_2, HCHO, SO_2, H_2O, Glyoxal, BrO and others along the line of sight between the instrument and the target like for the well-known long-path DOAS observations (but with much less expense). If tomographic arrangements are used, even two- or three-dimensional trace gas distributions can be retrieved. The basic assumptions of the proposed method are confirmed by test measurements across the city of Heidelberg.

OCIS codes: 010.1290, 280.1120, 300.1030

1. Introduction

One important issue in the field of air quality monitoring and the study of atmosphere processes is the possibility of mapping the temporal and spatial trace gas distribution with good resolution. Some techniques have been developed to measure the trace gas concentrations over cities or regions. Tomographic Long-Path Differential Optical Absorption Spectroscopy (DOAS) systems are one of the novel instruments developed in recent years and are successfully used for the determination of a variety of trace gases in the visible and the UV region.[1-3]

Another important technique that allows tomographic measurements is the Light Detection And Ranging (LIDAR). In this case the light source is a laser and the information is obtained by means of the measured back scattered light as a function of time.[4-6] Both techniques are well established and have been successfully applied but suffer from the drawback that their operation is very expensive and require extensive personpower for operation. Another drawback of LIDAR measurements is that they are usually limited in their coverage of multiple species.

Multi-AXis-DOAS (MAX-DOAS) is a further development combining features of the well-known zenith-scattered light DOAS[7-11] and Long-Path DOAS.[12-14] It is a novel technique, which allows quantitative measurements of atmospheric trace gases like e.g. NO_2, HCHO, BrO, Glyoxal, SO_2, and aerosol properties.[15-24] It combines the inherent advantage of spectroscopic techniques like real time measurements and absolute calibration through molecular parameters with a simple set-up and cost-effective operation.

The calculation of path-average trace gas concentration from active long-path DOAS observations is straightforward. In the case of zenith-scattered light DOAS or MAX-DOAS measurements using scattered sunlight, where the radiation travels along multiple paths, a detailed modeling of the radiation transfer in the atmosphere is required.[8, 9, 22, 23, 25]

Here we propose the use of MAX-DOAS observations of targets which are illuminated by sunlight. Two general possibilities exist: either bright targets can be used; then a substantial (or even the major) fraction of the received light is reflected by the target. Alternatively, black targets can be used; then the received light is solely scattered within the air volume between the instrument and target. In either case, the novel technique combines the advantages of both, passive and active systems: no artificial light sources involving relatively complicated optical set-ups are needed. In addition, the interpretation of the observations can be referred to well-defined light paths and even allows tomographic inversions.[26]

The main limitations of the method are the restriction to wavelengths >300 nm and to daytime. In particular, most aromatic compounds and night-time chemistry cannot be investigated. However, there is a large class of species including NO_2, HCHO, SO_2, H_2O, Glyoxal, BrO and others that can be detected.

The paper is organized as follows: In the next Section we introduce the proposed measurement technique, describe the composition and information content of the measured light, and the specific requirements and subsequent steps of the spectral analysis. In the following Section the various measurements strategies and possible results (including tomographic techniques) are described. In Section 4 first measurement examples are presented. Finally, we summarize our findings and give recommendations for basic and advanced measurements strategies and for the specific design of advantageous experimental set-ups.

2. MAX-DOAS observations of illuminated targets

In many aspects, tomographic MAX-DOAS observations can be treated very similarly to tomographic DOAS measurements using artificial light sources and well-defined light paths.[1-3, 27] In particular, we will show in this study, that tomographic MAX-DOAS eventually yields an

intermediate product very similar to active long-path DOAS: the path-integrated (or average) trace gas concentration between the instrument and the target. However, there are also two fundamental differences: first, MAX-DOAS observations use the sun, which is an extraterrestrial light source. Second, atmospheric scattering processes between the instrument and the target can also contribute to the measured signal. In the following Sections the resulting effects and their correction are described in detail.

2.A Tomographic MAX-DOAS measurements

MAX-DOAS observations directed to targets illuminated by sunlight receive photons which have traversed two basic sections in the atmosphere: the distance between the top of the atmosphere and the target, and the distance between the target and the instrument (see Fig. 1).

Depending on the investigated problem, the properties of the measuring site and the number of instruments and targets, a large variety of measurement geometries can be developed. In the simplest case one instrument is directed to one target; then the average concentration between the instrument and the target can be derived. Targets at different distances or altitudes allow the retrieval of horizontal or vertical gradients (see Fig. 1). More-dimensional tomographic set-ups can even yield the spatial trace gas distribution.

Irrespective of the final inversion strategy, the basic quantity which is derived from the spectral DOAS analysis is the (differential) optical depth τ of a selected trace gas, from which the so-called slant column density (SCD) S, the trace gas concentration integrated along the light path L, can be derived by dividing it by the respective absorption cross section at the same wavelength:

$$S = \int_0^L \rho(l)dl = \frac{\tau(\lambda)}{\sigma(\lambda)} \quad (1)$$

It should be noted that for the DOAS analysis usually the so-called differential optical depth is analyzed, which - in the simplest case - is the difference of the optical depth at different wavelengths.[14,28] In analogy, also a differential cross section can be defined, which then has to be applied in Equation 1. They might e.g. indicate the difference of the absorption cross section (or optical depth) inside and outside an absorption band. For these differential quantities we will use the term τ' and σ' in the following.

The analyzed total SCD can be expressed as the sum of the partial SCDs of both sections introduced above (see Fig. 1):

$$S_{tot} = S_{Target} + S_{Atm} \quad (2)$$

Here S_{Target} is the trace gas concentration integrated between the instrument and the target; S_{Atm} is the trace gas concentration integrated between the target and top of the atmosphere. For many trace gases like NO_2, BrO, or O_3 a substantial or major fraction of the total atmospheric column is located in the stratosphere; for such trace gases, S_{Atm} will be independent from the MAX-DOAS viewing direction, because the absorption paths through the stratosphere are determined by the solar zenith angle. Even for trace gases located in the free or upper troposphere this assumption is valid with only small restrictions.

It should be noted that the sensitivity of the measurement for the trace gases between the instrument and the target strongly depends on the brightness of the target and the atmospheric conditions. Only for white targets, the measured SCD is almost similar to the true SCD S_{Target} (see below).

As we are interested in S_{Target}, we have to remove S_{Atm} from the total signal. This can be easily achieved and will be explained in Section 2.B. Another fundamental question is to determine the sensitivity of the measurement for the trace gas between the instrument and the target, in particular the dependence of the sensitivity as a function of the distance from the instrument. For an ideal measurement the sensitivity would be constant along the light path between the instrument and the target like e.g. for traditional long-path DOAS observations. We will show below that indeed for many cases the sensitivity can be expressed as a simple functional expression of the distance from instrument. For bright targets, for example, the sensitivity becomes similar to that for long-path DOAS observations. Nevertheless, in general, this sensitivity decreases with distance from the detector, because additional sunlight is scattered into the line of sight of the instrument (see Fig. 1). For the correct interpretation of the measurement, this sensitivity has to be characterized (see Section 2.C) and corrected. If no simple correction is possible, radiative transfer modeling has to be applied (see Section 2.D).

2.B Removal of the signal from the region between the target and top of the atmosphere (S_{Atm})

The correction of the partial SCD between target and the top of the atmosphere (S_{Atm}) can be easily (and quasi automatically) achieved by two procedures. The main aspect of both methods is that for the DOAS analysis of scattered sunlight a so-called Fraunhofer spectrum has to be included for the correction of the strong solar Fraunhofer lines.[8,9,11,23] For this purpose usually a measurement taken with the same instrument but under different measurement conditions (e.g. at low solar zenith angle) is used. Since this Fraunhofer spectrum contains not only the solar Fraunhofer lines but also atmospheric absorptions, the result of the spectral DOAS analysis is the difference between the SCDs of the measurement and the Fraunhofer spectrum. The trick for the

correction of signal from between the target and the top of the atmosphere (S_{Atm}) is to select a Fraunhofer spectrum, which only contains S_{Atm}. This can easily be achieved by two simple approaches. The first approach is to point the telescope of the instrument toward the zenith. It then receives photons which have traversed almost similar paths as those between the target and the top of the atmosphere. Especially for trace gases which (in addition to the boundary layer) are only located in the stratosphere, a zenith-scattered spectrum is already sufficient for the correction of S_{Atm}. If trace gases are also located in the free troposphere it might be, however, better to choose a refined approach. For the measurement of the Fraunhofer spectrum the telescope should then be directed to a target close to the instrument, which has similar properties compared to the real targets. Especially the orientation (angle of the reflecting surface with respect to the instrument and the sun) and the reflectivity (albedo) of the nearby target should be similar to the target at far distance. This procedure ensures that the photon paths in the lower free troposphere (and thus the S_{Atm}) of both, the actual measurement and the Fraunhofer spectrum, are almost identical.

In some cases it might be already sufficient to use a measurement from one (far) target (e.g. measurement D in Fig. 1) as the Fraunhofer spectrum for the analysis of a measurement from another (far) target which is placed in the same direction, but at a different distance (e.g. measurement C in Fig. 1). Then the resulting S_{Target} is the integrated trace gas concentration along the path between both targets.

2.C Sensitivity of the measurement for trace gases between the instrument and the target

For the correct interpretation of the trace gas absorption determined by the DOAS analysis the sensitivity of the MAX-DOAS observation for the trace gas between the instrument and the

target (e.g. as a function of the distance from the instrument) has to be known. We will show below that for many cases simple functional expressions for this dependence can be found.

The light received by the telescope $I(\lambda, L)$ contains two parts (see Fig. 2):

$$I(\lambda, L) = I_{Atmos}(\lambda, L) + I_{Target}(\lambda, L) \tag{3}$$

where $I_{Target}(\lambda, L)$ is the measured radiance caused by the reflected sunlight by the target, and $I_{Atmos}(\lambda, L)$ the radiance caused by the scattered sunlight into the line of sight of the telescope between the target and the instrument.

The light scattered or reflected into the line of sight of the instrument will be attenuated by scattering and absorption (on molecules and aerosols) between the point of reflection or scattering and the instrument. Since we are interested in the differential trace gas absorptions, we will in the following use the term absorption only for the high frequency part of the trace gas absorption. Other extinction processes which vary only slowly with wavelength we will refer to as extinction processes. While these processes contain also any broadband absorption of trace gases, for most measurements, extinction by aerosols and molecules between the target and the instrument will contribute the dominant part. For simplicity and without restriction of the general case, we will reduce all considerations to one absorbing trace gas. With these assumptions the measured radiance depends on the following quantities:

$$I(\lambda, L) = \int_0^L i_{scatt}(\lambda, l) \cdot e^{-\tau'_{abs}(\lambda, l)} \cdot e^{-\tau_{ext}(\lambda, l)} dl \; + \; I_{refl}(\lambda, A) \cdot e^{-\tau'_{abs}(\lambda, L)} \cdot e^{-\tau_{ext}(\lambda, L)}, \tag{4}$$

where $i_{scatt}(\lambda,l)$ is the radiance per unit length (in units: $Wm^{-3}sr^{-1}$) due the photons scattered into the field of view at the distance l and wavelength λ., and $I_{refl}(\lambda,A)$ is the due to the photons

reflected from the target into the field of view, with A being the albedo of the target. $\tau_{ext}(\lambda,l)$ is the optical depth of the extinction between the instrument and distance l: $\tau_{ext}(\lambda,l)=\int_0^l k_{ext}(\lambda,l)dl$ with $k_{ext}(\lambda,l)$ the extinction coefficient for Rayleigh and aerosol scattering (and all additional broad band extinction processes) at the distance l and wavelength λ. $\tau'_{abs}(\lambda,l)$ is the differential optical depth of the trace gas absorption between the instrument and distance l: $\tau'_{abs}(\lambda,l)=\int_0^l \sigma'(\lambda)\cdot\rho(l)dl$ with $\sigma'(\lambda)$ the differential absorption cross section of the trace gas of interest at wavelength λ and $\rho(l)$ the trace gas density at the distance l.

In general, most of the quantities in Equation 4 vary with the distance from the instrument. Usually, e.g. the trace gas concentration and the aerosol scattering are not constant along the line of sight. In addition, usually also the solar radiation scattered into the field of view will depend on the distance from the instrument because of several reasons: first, the incoming solar radiation can vary because of shielding by heterogeneous clouds or aerosols. Second, the scattering coefficient can vary due to changing aerosol concentrations and/or aerosol properties. Third, changes in the ground albedo can lead to variations of the solar radiation scattered into the field of view of the instrument.

Because of these variations, usually there is no simple solution of Equation 4 and radiative transfer modeling has to be applied. Nevertheless, for many cases the above-mentioned quantities vary only slightly or can be assumed to be constant over the line of sight between the instrument and the target. For example, the sky might be clear or covered by a homogeneous cloud cover, and the ground albedo and the aerosol properties might not change substantially

between the instrument and target. Then, the scattered radiance will not vary as a function of distance between the instrument and the target, and i_{scatt} can be put in front of the integral. If also the aerosol extinction and the trace gas absorption are constant over the line of sight, their optical depths become linear functions of the distance:

$$\tau_{ext}(\lambda, l) = k_{ext}(\lambda) \cdot l$$

$$\tau'_{abs}(\lambda, l) = \sigma'(\lambda) \cdot \rho \cdot l = k'_{abs}(\lambda) \cdot l$$

Then Equation 4 reduces to:

$$I(\lambda, L) = i_{scatt}(\lambda) \int_0^L e^{-k_{ext}(\lambda) l} \cdot e^{-k'_{abs}(\lambda) l} dl \; + \; I_{refl}(\lambda, A) \cdot e^{-k_{ext}(\lambda) L} \cdot e^{-k'_{abs}(\lambda) L} \tag{5}$$

and finally to:

$$I(\lambda, L) = i_{scatt}(\lambda) \cdot L \frac{1 - e^{-[(k_{ext}(\lambda) + k'_{abs}(\lambda)) L]}}{(k_{ext}(\lambda) + k'_{abs}(\lambda)) \cdot L} \; + \; I_{refl}(\lambda, A) \cdot e^{-k_{ext}(\lambda) L} \cdot e^{-k'_{abs}(\lambda) L} \tag{6}$$

In the following we will use the general form for the optical depth (of extinction and trace gas absorption) for variable concentration fields of trace gases and aerosols.

Our goal is to determine the differential optical depth of the absorbing trace gas. For that purpose within the DOAS analysis the negative logarithm of the ratio of the measured radiance with and without trace gas absorption has to be formed in order to invert the Beer Lambert law (see Equation 1). We will call the differential optical depth calculated in this way the "measured differential optical depth" ($\tau'_{meas}(\lambda, L)$):

$$\tau'_{meas}(\lambda, L) = -\ln\left[\frac{i_{scatt}(\lambda)\int_0^L e^{-\tau_{ext}(\lambda,l)} \cdot e^{-\tau'_{abs}(\lambda,l)} dl \; + \quad I_{refl}(\lambda, A) \cdot e^{-\tau_{ext}(\lambda,L)} \cdot e^{-\tau'_{abs}(\lambda,L)}}{i_{scatt}(\lambda)\int_0^L e^{-\tau_{ext}(\lambda,l)} dl \; + \quad I_{refl}(\lambda, A) \cdot e^{-\tau_{ext}(\lambda,L)}}\right] \tag{7}$$

It is important to note here that in the DOAS analysis the term in the denominator (without the (differential) trace gas absorption) is approximated by a) the Fraunhofer spectrum (representing the Fraunhofer lines, see Section 2.B.)) and a low order polynomial (representing the broad-band effects of atmospheric scattering and absorption).[11]

In the case of a strong absorber ($\tau'_{abs}(\lambda, l) >> 0$) there appears to be no simple solution possible for Equation 7 (a strong absorber of interest might be e.g. water vapour). However, for weak absorbers ($\tau'_{abs}(\lambda, l) << 1$) Equation 7 can be linearized by expanding the logarithmic and exponential functions:

$$\tau'_{meas}(\lambda, L) \approx \frac{\left[i_{scatt}(\lambda)\int_0^L e^{-\tau_{ext}(\lambda,l)} \cdot \tau'_{abs}(\lambda, l) dl \; + \quad I_{refl}(\lambda, A) \cdot e^{-\tau_{ext}(\lambda,L)} \cdot \tau'_{abs}(\lambda, L)\right]}{i_{scatt}(\lambda)\int_0^L e^{-\tau_{ext}(\lambda,l)} dl + \quad I_{refl}(\lambda, A) \cdot e^{-\tau_{ext}(\lambda,L)}} \tag{8}$$

It follows that the differential optical depth of the trace gas absorption is the average of the differential optical densities of the total (infinite) number of contributing light paths weighted by their respective radiances.[25] From radiative transfer simulations we could estimate the error for values of $\tau'_{abs}(\lambda, l) >> 0$. For $\tau'_{abs}(\lambda, L)$ = 1 the relative error of the observed differential optical depth from the intensity weighted average is still < 10% (this is true only if the differential absorption structure can be resolved by the instrument).

If also the extinction due to scattering can be neglected ($\tau_{ext}(\lambda,l) << 1$) then also the exponential function for the extinction can be expanded and Equation 8 becomes:

$$\tau'_{meas}(\lambda,L) \approx \frac{\left[i_{scatt}(\lambda) \int_0^L \tau'_{abs}(\lambda,l)dl \; + \; I_{refl}(\lambda,A) \cdot \tau'_{abs}(\lambda,L) \right]}{i_{scatt}(\lambda) \cdot L \; + \; I_{refl}(\lambda,A)} \tag{9}$$

From radiative transfer simulations we could also estimate the error if $\tau_{ext}(\lambda,l) >> 0$. For $\tau_{ext}(\lambda,L)$ = 1 the relative error of the observed differential optical depth from the intensity weighted average is still < 20%.

Now several simple cases can be distinguished depending e.g. on the chosen wavelength range, the atmospheric conditions, and the brightness of the target (see following sub-Sections). One important question is, how sensitive the observation is for trace gases between the instrument and the target. For an 'ideal' observation the sensitivity would be constant along the line of sight. That means that an air mass with a given concentration of a trace gas would cause the same measured differential optical depth $\tau'_{meas}(\lambda,L)$ independent from the position between the instrument and the target. The measured differential optical depth $\tau'_{meas}(\lambda,L)$ is similar to the (true) differential optical depth $\tau'_{abs}(\lambda,L)$ integrated over the path segment *L* between the target and the receiving telescope (see Fig. 2).

To gain more direct insight, we can especially construct the ratio between the observed differential optical depth $\tau'_{meas}(\lambda,L)$ and the true differential optical depth $\tau'_{abs}(\lambda,L)$, which defines what we will call the "sensitivity" (*R*) of the measurement:

$$R(L) = \frac{\tau'_{meas}(\lambda,L)}{\tau'_{abs}(\lambda,L)} = \frac{S_{meas}(\lambda,L)}{S_{Target}(L)} \tag{10}$$

with $S_{meas}(\lambda, L)$ derived from $\tau'_{meas}(\lambda, L)$ using Equation 1.

After the sensitivity R is determined (either from Equation 9, if the absorption and extinction is weak, or from radiative transfer calculations, see Section 2.D.), the measured SCD $S_{meas}(\lambda, L)$ can be transformed into the desired true SCD ($S_{Target}(\lambda, L) = \frac{\tau'(\lambda, L)}{\sigma'(\lambda)}$), which can then be used for the subsequent (tomographic) inversion steps.

The sensitivity can be determined for the whole path between the instrument and the target or for any subdivided path segments. For an 'ideal' observation (like e.g. for the traditional long-path DOAS measurements) the sensitivity will be unity.

In the following we discuss three limiting cases for topographic targets of high and low reflectivity ('white and black' targets), respectively. The corresponding contributions of the measured radiance and sensitivity as a function of distance from the instrument are summarized in Fig. 3.

2.C.1 'White targets': $I_{Target} >> I_{Atmos}$

For many cases the radiance reflected by the target will be much higher than that due to scattering between the instrument and the target. This might be the case for an optically thin atmosphere ($\tau_{ext}(\lambda, l) << 1$), e.g. for a short horizontal light path, low aerosol load, long wavelength) and bright targets (e.g. white painted walls). Then almost all of the received light is reflected from the target and has thus traversed the full distance between detector and target (see Fig. 3a). Equation 9 reduces to

$$\tau'_{meas}(\lambda, L) \approx \frac{\left[I_{refl}(\lambda, A) \cdot \tau'_{abs}(\lambda, L)\right]}{I_{refl}(\lambda, A)} = \tau'_{abs}(\lambda, L) \qquad (11)$$

It follows that the sensitivity R is unity like that for 'traditional' long-path DOAS observations; furthermore it is not dependent on the distance of the trace gas from the detector. The analyzed S_{meas} can be directly used for any subsequent inversion processes. In the simplest case the average trace gas concentration between the instrument and the target can be derived as $\overline{\rho} = \frac{\tau'_{abs}(\lambda, L)}{\sigma'(\lambda) \cdot L}$.

2.C.2 'Black targets': $I_{Target} << I_{Atmos}$

If the target is perfectly black, only light scattered between the instrument and the target is received. Equation 9 reduces to

$$\tau'_{meas}(\lambda, L) \approx \frac{\left[i_{scatt}(\lambda) \int_0^L \tau'_{abs}(\lambda, l) dl \right]}{i_{scatt}(\lambda) \cdot L} = \frac{1}{L} \int_0^L \tau'_{abs}(\lambda, l) dl \qquad (12)$$

Now, the sensitivity for any subdivided path segments decreases linearly from 1 at the instrument to zero at the target (see Fig. 3b). If the trace gas concentration is uniform along the line of sight $\tau'_{meas}(\lambda, L) \approx \frac{\tau'_{abs}(\lambda, L)}{2}$ and the sensitivity R for the total path between the instrument and the target is 0.5.

2.C.3 Mixed cases: $I_{Target} \approx I_{Atmos}$

For many cases the radiance reflected by the target and scattered towards the instrument from between the instrument and the target will be of similar magnitude. If the trace gas concentration is uniform between the instrument and the target, Equation 9 reduces to:

$$\tau'_{meas}(\lambda, L) \approx \frac{1/2 \cdot i_{scatt}(\lambda) \cdot L + I_{refl}(\lambda, A)}{i_{scatt}(\lambda) \cdot L + I_{refl}(\lambda, A)} \cdot \tau'_{abs}(\lambda, L) \quad (13)$$

and the sensitivity $R = \frac{1/2 \cdot i_{scatt}(\lambda) \cdot L + I_{refl}(\lambda, A)}{i_{scatt}(\lambda) \cdot L + I_{refl}(\lambda, A)}$ will be between 0.5 and unity, depending on the relative contributions of $i_{scatt} \cdot L$ and I_{refl}.

2.C.4 Hazy Conditions: $\tau_{ext}(\lambda, l) >> 0$

In the case of an optically thick atmosphere with respect to Rayleigh and aerosol scattering (e.g. long horizontal light path, high aerosol load, small wavelength) the received light is mainly scattered from distances not far away from the detector (see Fig. 3c). If the extinction coefficient of the aerosol scattering is known, Equation 8 can be solved. While the Rayleigh scattering coefficient can be directly derived from the air pressure, that for aerosol scattering is, unfortunately, usually unknown. However, an elegant procedure for the determination of the aerosol scattering properties is to directly investigate the MAX-DOAS measurements themselves.[29,22-24] Since the atmospheric concentration of the oxygen molecule (O_2) and dimer ($(O_2)_2$) is known, the deviation of the measured O_2 and O_4 absorptions from those of a pure Rayleigh atmosphere can be directly attributed to the additional scattering by aerosols and accordingly the necessary aerosol scattering properties can be determined; additional information can be derived from the observed relative radiance and the strength of the Ring effect.[23] For very strong aerosol extinction (e.g. for foggy conditions) the instrument cannot 'see' the target anymore. The sensitivity of such observations is then limited to trace gases very close to the detector. Equation 8 reduces to:

$$\tau'_{meas}(\lambda, L) \approx \frac{i_{scatt}(\lambda)\int_0^L e^{-\tau_{ext}(\lambda,l)} \cdot \tau'_{abs}(\lambda,l)dl}{i_{scatt}(\lambda)\int_0^L e^{-\tau_{ext}(\lambda,l)}dl} \quad (14)$$

2.D Radiative transfer modeling

As shown in Section 2.C., the sensitivity of MAX-DOAS observations using illuminated targets can for many cases be determined and corrected in very simple ways (see especially Sections 2.C.1. and 2.C.2.). For the set-up of MAX-DOAS observation geometries it should thus be the aim to ensure that these conditions are actually met. One general recommendation is to use either an almost black or a bright target.

Nevertheless, in general, no simple solution of Equation 8 might be possible and it has to be solved by numerical simulation of the atmospheric radiative transfer.[9,25] Even, if the requirements of an almost black or bright target are met, radiative transfer modeling might still be needed because of the following reasons:

a) The trace gas absorption $\tau'_{abs}(\lambda,l)$ is strong (>>0) like e.g. for H_2O or O_2

b) The optical depth of Rayleigh- and aerosol scattering $\tau_{ext}(\lambda,l)$ is large (>>0). This can be the case for measurements at small wavelengths where the probability of Rayleigh-scattering is large, or for high aerosol concentrations (haze or fog)

c) The radiance scattered into the line of sight between the instrument and the target varies with distance from the instrument. This might be e.g. the case if the incoming solar radiation is non-uniform due to a varying cloud cover above the line of sight. In addition, a changing ground albedo or changing aerosol properties between the instrument and the target might also cause such variations.

d) The above effects might become even more important if the trace gas distribution itself is not constant along the line of sight.

In analogy to the well-known calculation of air mass factors[9,25], the numerical simulation of the sensitivity *R* can be performed in the following way:

a) In a first step a model scenario including the detector properties (field of view, viewing direction, wavelength, etc.), the geometrical situation (topography, distance and orientation of the target, solar zenith and azimuth angle, etc.), the spatial distributions of the trace gas and aerosol properties (concentration, extinction coefficient, phase function, etc.) as well as surface properties (albedo, bidirectional reflection function, etc.) is set up. A suitable discretization has to be chosen.

b) A geometrical path segment (e.g. the whole path between the instrument and the target) is selected. S_{Target} is calculated by integrating the trace gas concentration along this path segment.

c) The radiance received at the instrument with and without the trace gas of interest is calculated (this represents the radiances of the numerator and denominator of Equation 7). Taking the negative logarithm of the ratio of both quantities (Equation 7) yields the differential optical depth of the trace gas of interest $\tau'_{meas}(\lambda, L)$.

d) From S_{Target} and $\tau'_{meas}(\lambda, L)$ the sensitivity is calculated using Equations 1 and 10:

$$R(L) = \frac{\tau'_{meas}(\lambda, L)}{S_{Target}(L) \cdot \sigma'(\lambda)} \tag{15}$$

It should be noted that in general not all input parameters for the correct simulation of the atmospheric radiative transfer (step a) are known. In particular, the aerosol scattering might be unknown. The great advantage of MAX-DOAS measurements is that such information on the aerosol scattering (and additional parameters) can be directly retrieved from the simultaneously

measured absorptions of the oxygen molecule O_2 and the dimer O_4 and additional measurement quantities.[23, 29]

It might be also interesting to note that for some cases the sensitivity as defined in Eq. 10 exceeds unity (in contrast to long-path DOAS observations). This will in particular be the case if multiple scattering (e.g. for high aerosol load and over bright surfaces) leads to a path length enhancement compared to the geometrical length.[29-32]

Especially for tomographic inversion strategies it will be important to subdivide the total path between the instrument and the target into partial segments within the selected discretization scheme.[2, 27] Accordingly, the sensitivity R_i for these sub segments can be determined using the same modeling approach as outlined above. For the partial SCDs and the sensitivities the following relations are valid:

$$S_{meas} = \sum_i S_{meas,i} \tag{16}$$

$$S_{Target} = \sum_i S_{Target,i} \tag{17}$$

$$S_{Target,i} = \frac{S_{meas,i}}{R_i} \tag{18}$$

3. Experimental requirements and inversion strategies

The practical implementation of the measurements described above is rather straightforward, especially if based on the now widespread Mini–MAX-DOAS instruments.[18, 33] Here some notes will be made. First, a 'natural' white target may be snow cover, a glacier, or a brightly painted wall of a building. In addition, 'artificial' white targets may be created by painting surfaces or adding white (plastic) sheets like e.g. spectralon. It should be kept in mind that high reflectivity

in the visible may not guarantee high reflectivity in the near UV or infrared spectral ranges. Second, 'natural' black surfaces may be low reflectance surfaces like vegetation or – more importantly – cavities of any kind. In urban environments this might be open windows or other structures opening relatively small apertures to large cavities. These cavities ('hohlraum') form almost perfect black objects, since radiation entering the cavity is reflected from the inner surfaces many times before leaving again.

Another point to watch is the field of view of the instrument. Customary Mini-MAX-DOAS spectrometer telescope combinations have fields of view of the order of 1 degree. For instance a fiber (connecting telescope to spectrometer) of d = 0.3mm diameter and a F/4 telescope (10 mm aperture, f = 40 mm) would result in a field of view of d/f = 0.0075 radian or 0.43 degrees. A target at e.g. 4 km distance would have to have a diameter of 30 m. Thus in general, Mini-MAX-DOAS instruments are not ideally suited for the applications described here. Fortunately, however, passive instruments can easily be modified to fulfill the requirements by adding a somewhat larger telescope. In the above example a still quite compact optics with 100mm aperture and f = 400 mm would require a target diameter of only 3 m at 4 km distance.

Because of their simple experimental requirements, MAX-DOAS observations can be performed in very flexible geometries. In particular, it is very easy to point one instrument towards several well suited targets. Moreover, because the instruments are small and can be operated automatically, several instruments can be used simultaneously, making e.g. more dimensional tomographic geometries possible. Depending on the number of instruments and targets, results of largely varying complexity can be derived. A description of the basic set-ups is given in this Section.

3.A Determination of the average concentration along the light path

In the simplest case, only one instrument and a single target is used. This simple set-up is very similar to the well-known long-path DOAS and it allows the retrieval of the average trace gas concentration along the line of sight between the instrument and the target. It should be noted, that in cases of low visibility such measurements are only sensitive to the trace gas concentration close to the instrument. However, under such conditions, the weak signal received from long-path observations usually does not allow a reasonable data analysis anymore.

3.B One-dimensional gradients

There are two basic possibilities for the retrieval of one-dimensional gradients from MAX-DOAS observations of sun-illuminated targets. Either targets at the same location but with different reflectivities are observed, or the instrument is pointed to several targets placed in the same direction, but at different distances.

3.B.1 Alternating view at 'white' and 'black' target at the same distance

As shown in Sections 2.C.1. and 2.C.2. the sensitivity close to the target strongly depends on the brightness of the target. It is almost unity for a bright target and almost zero for a black target. Thus from alternating observations of a bright and black target at the same location, information on the horizontal trace gas distribution can be derived. This possibility can be illustrated with some simple examples: if e.g. the S_{meas} is the same for the observation of the black and the bright target, then substantial concentrations of the trace gas must be located only very close to the instrument. If S_{meas} for the observation of the black target is half that of the bright target, then the trace gas concentration should be almost constant along the line of sight. If the S_{meas} for the observation of the black target is zero and that of the bright target is >0, then the trace gas must

be located very close to the target. Observations of alternating view on a bright and black target can be easily achieved observing e.g. a black open window or the white wall of a building.

3.B.2 Determination of horizontal gradients using targets at different distances

If one instrument is pointed to different targets placed in the same direction but at different distances (see Fig. 1), the analyzed S_{meas} represent the integrated trace gas concentrations of the different sub-sections. From a simple linear inversion a one-dimensional gradient can be derived.

3.B.3 Determination of vertical gradients using targets at different altitudes

One could think that a similar strategy as shown in Section 3.B.2. could also be applied to derive one dimensional gradients in vertical direction. For example, an instrument placed at the bottom of a high tower or a steep hill slope could be pointed at targets at different altitudes. Unfortunately, for such arrangements, S_{Atm} will in general also depend on the altitude of the respective target. In general, S_{Target} will increase in the same way as S_{Atm} decreases if targets at increasing altitude are observed. Thus, S_{tot} (Equation 2) will be the same for all measurements and no altitude information can be extracted from this simple setup. Fortunately, there are two basic alternatives to overcome this problem: First, instead of putting the instrument at the ground, it could be placed on top of the tower or the hill and directed to targets located below. Then, both S_{Atm} and S_{Target} will increase if the altitude of the target decreases and it is possible to retrieve information on the vertical profile.

A second possibility is to place the instrument at the bottom, but at a substantial distance apart from the location of the tower or hill (see Fig. 1). Then, the light path through a given height layer between the instrument and the target will be enhanced because of the slant

geometry and S_{Target} and S_{Atm} will change in a different way if targets at different altitudes are observed. Again, it will be possible to extract information on the vertical trace gas distribution. Nevertheless, it should be noted that this procedure can only be applied correctly if the horizontal gradients are small compared to the vertical ones.

3.C Higher-dimensional (tomographic) inversion

With several instruments pointed to various targets, a multitude of (at least partly) crossing light paths can be created. Such set-ups can be arranged in two or even three dimensions. For such arrangements, it will be of greatest benefit if the instrumental expense of tomographic MAX-DOAS observations is very low compared to active long-path DOAS observations, because no artificial light sources have to be operated and no mirrors have to be set up. Thus the acquisition and operation of tomographic MAX-DOAS observations will be much cheaper compared to conventional long-path DOAS observations. Because of these advantages, it will be much easier to set up a larger number of instruments and to create a significantly higher number of light paths. This will allow enhancement of the spatial resolution of such tomographic measurements and will in particular reduce the necessity of appropriate a-priori information.

Tomographic inversion schemes first require the setup of a suitable inversion grid. Then, the sensitivities of the various light paths crossing the boxes of this grid have to be calculated. If bright targets are observed it will be indeed possible for many cases (with bright targets, see Section 2.C.1.) to achieve sensitivities close to one; it follows that the problem can be treated simply in a geometrical way. In the general case, the observed S_{meas} for a given instrument and target will be composed of the partial $S_{Target,i}$ of the boxes through which the line–of-sight passes, weighted by the respective sensitivities. From Equations 16 to 18 it follows:

$$S_{meas} = \sum_i S_{Target,i} \cdot R_i \tag{19}$$

If the trace gas concentration within a given box is assumed to be constant, any partial $S_{Target,i}$ will be the product of the trace gas concentration and the length of the line-of-sight crossing the respective box (see Fig. 4). Accordingly, it is possible to create a linear system of Equations which can be represented by a matrix equation:

$$\vec{Y} = \mathrm{M} * \vec{X} \tag{20}$$

with $\vec{Y}$ representing the measurement vector consisting of the S_{meas} of all combinations of light paths between the various instruments and targets, $\vec{X}$ representing the state vector consisting of the concentrations of all boxes of the model grid which were crossed by any line of sight. The matrix M consists of the partial path lengths and the respective sensitivities for a given segment of a line of sight through a grid box.

The matrix has then to be inverted and Equation 20 to be solved to derive the trace gas concentrations in the boxes of the model grid. Depending on whether the problem is over- or underdetermined, also a-priori information might be used. The different methods to solve such inversion problems will not be discussed in more detail here. Appropriate methods can be found in existing literature.[2, 27, 34, 35]

4. Test measurements at Heidelberg

During the 21st of March 2005 measurements with a Mini-MAX-DOAS instrument were carried out on the roof of the Environmental Physics Department of the University of Heidelberg as a first case study. The Miniaturized Multi Axis Differential Optical Absorption Spectroscopy (Mini-MAX-DOAS) instrument used here, consists of an entrance optic (quartz lens, f = 40 mm,

d = 20 mm, field of view approximately 0.6°) coupled to a quartz fibre bundle, which transmits the light into a commercial miniature fibre optic spectrometer (OceanOptics Inc., USB2000) with a spectral resolution of 0.7 nm. This unit is placed inside a metal box which can be mounted on a tripod and can therefore be moved to point at different elevation angles between 0 and 180 degrees (from horizon to horizon). For a detailed description see Ref 36.

In order to reduce the dark current of the CCD and to stabilize the optical bench the complete USB2000 spectrograph was cooled to a temperature of +10 °C during the measurements. Stabilizing the temperature of the spectrometer and detector readout electronics also reduces the temperature drift of the electronic offset signal. To avoid water condensation the whole unit was made airtight and silica gel was added to keep the interior dry in case of leakage. The entire system (computer, cooling system, spectrometer and stepper motor) was operated with a car battery and controlled by a notebook. Data acquisition was performed by the software package DOASIS (see www.iup.uni-heidelberg.de/bugtracker/projects/doasis/).

It should be noted that these measurements are by far not sufficient to test all scenarios described in the preceding Sections. This should be the subject of subsequent detailed investigations. Here our aim was to test two basic assumptions of our new technique: first, can the trace gas absorption between the target and top of the atmosphere be removed from the measured total absorption with sufficient accuracy? Second, can spectra measured by pointing on targets be analyzed with standard analysis tools, like e.g. for the well known DOAS measurements of zenith scattered sunlight[11]? We tested these aspects by the analysis of the atmospheric NO_2, which in polluted regions is usually present in the troposphere and stratosphere.

Our instrument was pointed towards the hills of the nearby Odenwald, which are covered by green forest. Measurements were taken for two azimuth angles for which the telescopes were

directed to hill targets at different distances (see Fig. 5 and 6). For the first azimuth angle the hills were about 1.9 km away (we will refer to these observations as short path, sp); for the second azimuth angle they were about 3.3 km apart (we will refer to these observations as long path, lp, see Fig. 5 and 6). In addition, zenith-sky observations were performed to derive appropriate Fraunhofer spectra for the correction of S_{Atm}. The following measurement sequence was applied: 3 times short path (church), 2 times long path (castle), 3 times zenith sky, 3 times long path (castle), 3 times short-path (church) and 3 times zenith sky.

From the measured radiances and O_4 absorptions (see below), we conclude that our observations constitute a 'mixed case' as described in Section 2.C.3.

We performed two basic spectral analyses: First the spectra in the two directions were analyzed using a zenith-sky observation as Fraunhofer spectrum. For this case the analyzed NO_2 absorption represents the integrated NO_2 concentration between the instrument and the hill targets. According to the chosen directions we will refer to these SCDs as S_{sp} and S_{lp}. The details of the spectral DOAS analyses of NO_2 and O_4 are described in Table 1.

In a second analysis, the spectra of the long path were analyzed using the observations of the short path as a Fraunhofer spectrum. For this case the analyzed NO_2 absorption represents the difference between S_{sp} and S_{lp}. Since both targets are located in a similar direction, this difference can be seen as an approximation for the integrated NO_2 concentration along the 'line' between both targets. Results of the spectral NO_2 analysis are shown in Fig. 7 (see Ref. 42). The NO_2 SCDs for the different paths are presented in Fig. 8.

Two findings are important to note: first, both spectral analyses were possible using the standard DOAS technique for scattered sunlight observations.[11, 29, 43] Second, the resulting NO_2 absorptions of the second analysis were indeed the difference between the respective values of

the first analysis (as expected). From our investigation we conclude that spectra from different viewing direction may be well suited as Fraunhofer spectra. Although our simple test cases are by far not representative for the large variety of possible observational conditions, we see no obvious restriction against the free choice of appropriate Fraunhofer spectra, which is of great importance e.g. for the optimization of tomographic inversion schemes.

For the determination of the sensitivity R (Eq. 10) of our observations we investigated the measured radiance and the analyzed O_4 absorption. The observed radiance from the longer light path is about 30% larger than that measured at the shorter path. Thus we can conclude that the light reflected from the targets and that scattered from the atmosphere are of the same order of magnitude and our observation constitutes a 'mixed case' (see Section 2.C.3.). In order to determine the sensitivity R for our observations, we assume that the NO_2 concentration is constant along the light paths. This is of course an oversimplification, but here our main purpose is to show the applicability of our methods developed in Section 2.C. If we assume that i_{scatt} is constant throughout the observed area, and that the albedo of both targets is similar, we can determine the relative radiances of both the scattered and reflected light using the simple system of equations:

$$I_{lp} = i_{scatt} \cdot 3.3 \text{ km} + I_{refl}, \qquad I_{sp} = i_{scatt} \cdot 1.9 \text{ km} + I_{refl} \tag{21}$$

With $I_{lp} = 1.3 \cdot I_{sp}$ we find $i_{scatt} = 0.36 \cdot I_{refl} \cdot 1/km$.

Thus for the short and the long light path, the relative contributions of the scattered and reflected light are 40% and 54%, respectively. According to Equation 13, we calculate sensitivities of $R_{sp} = 0.8$ and $R_{lp} = 0.73$ for the short and the long light path, respectively. The results are also confirmed by the measured O_4 absorption (analyzed for the absorption bands at

360 nm and 380nm[38]). The measured difference between the O_4 SCDs of the two light paths was found to be between 1.5×10^{42} molec^2/cm^5 and 2.7×10^{42} molec^2/cm^5 (the units refer to the fact that the O_4 concentration is expressed with respect to the square of the O_2 concentration[44]), in good agreement with the value calculated for the conditions of our measurements (2.4×10^{42} molec^2/cm^5).

The true S_{Target} can now be calculated according to Equation 18. If they are subsequently divided by the path lengths, the average NO_2 concentration is derived. The results of these different steps are summarized in Table 2.

5. Conclusions and Outlook

We have introduced a novel technique to measure the near-surface distribution of atmospheric trace gases using a Multi-Axis-Differential Absorption Optical Spectroscopy (MAX-DOAS) pointed to non-reflecting surfaces or bright targets placed at known distances from the measuring device, which are illuminated by sunlight. From such observations it is possible to extract the partial absorption which took place along a well-defined absorption path between the instrument and the target and it is possible to retrieve the concentration of trace gases like e.g. NO_2, HCHO, SO_2, H_2O, BrO, like the well-known long-path DOAS observations (but with much less expense). Depending on the number of instruments and targets, results of different complexity can be derived: the use of one instrument and one target allows the derivation of the average trace gas concentration. If tomographic arrangements are used, more dimensional gradients can be retrieved. The proposed method is very simple, since it needs no artificial light source or mirrors, has low power requirements, and can be operated automatically. Besides these fundamental possibilities of the new method we also investigated several important details of the data analysis. We proposed two simple ways to remove the trace gas absorption between the

target and the top of the atmosphere from the total signal which is the prerequisite for the extraction of the signal for the path between the instrument and the target. In addition, we investigated the composition and information content of the measured light and we determined the sensitivity as a function of various measurement conditions like brightness of the target or atmospheric visibility. We showed that for selected measurement conditions (e.g. bright target and high visibility) a very simple (geometric) interpretation (like for the well-known long-path DOAS observations) is possible. For more complex situations (e.g. low visibility and spatial gradients of aerosol scattering) radiative transport modeling has to be applied. We presented a general procedure describing how this can be successfully applied. Of special importance here is that from the measurement itself (from simultaneously observed O_2 and O_4 absorptions as well as radiance and Ring effect) information on important quantities like aerosol scattering can be derived. We presented possible standard set-ups and inversion strategies for the retrieval of one and more-dimensional trace gas distributions.

Because tomographic MAX-DOAS observations need no artificial light sources and can be operated automatically they can be set up and operated with low expense. Thus very flexible and complex arrangements using several instruments and targets can be realized. Finally we presented prototype MAX-DOAS measurements at Heidelberg pointed to illuminated targets at nearby hills, which confirmed all basic assumptions of the method.

One major limitation of tomographic MAX-DOAS observations is that sunlight will be restricted to hours of daylight and to wavelengths >300 nm. Thus it will not be possible to investigate the night-time chemistry. In addition, many species of interest, like e.g. many aromatic compounds, can not be observed.

From our theoretical and practical investigations we can give the following recommendations for the application of the novel method:

-It is advantageous to aim for situations with high visibility and either bright or completely black targets. Such set-ups largely simplify the interpretation of the measurements.

-If more than one target is used, it is advantageous that all targets have similar orientation and albedo.

-The spectral range of the measurements should be chosen such that it contains at least one absorption band of O_4 or O_2. From these measurements (together with the radiance and the Ring effect) e.g. the influence of aerosol scattering can be analyzed and corrected.

-For species with very strong absorptions (like e.g. H_2O) a wavelength range with rather weak absorption bands should be chosen in order to minimize any non-linearities of the inversion procedure. Alternatively, such species could be observed over short absorption paths.

-If small targets (e.g. open windows at large distance) are observed, the field of view of the instrument has to be small. To ensure a high signal to noise ratio, relatively large telescope will be required.

-Besides the more obvious geometrical setups as discussed in Section 3, it might be important to propose some additional interesting geometries. One possibility is to install an instrument on top of a tower and systematically 'scan' the area of a city or factory below. Another possibility would be to arrange lines of sight over cities or other sources which are located in a deep valley or basin. It might then be possible to estimate the total emission from the basin. Another interesting option would be to place an instrument on a high mountain and to observe a target on a neighboring mountain. Depending on the altitude of the mountains, even measurements within the free troposphere could be realized. Because of the low air pressure at high altitudes such

measurements could be made over very large distances and will thus be very sensitive even to small trace gas concentrations (like e.g. for BrO in the free troposphere).

-Recently it has been shown that also in the near IR spectral range atmospheric species could be analyzed by absorption spectroscopy.[45-47] Because of the low probability of Rayleigh scattering in this spectral range, the light paths could extend over very long distances. It will be in particular possible to retrieve atmospheric CO and CH_4 from such observations.

Acknowledgements

E. F. thanks the German Academic Exchange Service (DAAD) for partially supporting this research.

References

1. Veitel H., B. Kromer, M. Mößner, and U. Platt, "New techniques for measurements of atmospheric vertical trace gas profiles using DOAS," *Environmental Science and Pollution Research* **special issue 4**, 17-26 (2002).

2. Laepple, T., V. Knab, K.U. Mettendorf, and I. Pundt, "Long-path DOAS tomography on a motorway exhaust plume: Numerical studies and application to data from the BAB II campaign," *Atmos. Chem. Phys.* **4,** 1323-1342 (2004).

3. Pundt, I., K.U. Mettendorf, T. Laepple, V. Knab, P. Xie, J. Lösch, C. v. Friedeburg, U. Platt, and T. Wagner, "Measurements of trace gas distributions using Long-path DOAS-Tomography during the motorway campaign BAB II: experimental setup and results for NO_2," *J. Atmos. Environ.* **39,** 967-975 (2005).

4. Collis, R.T. H., "Lidar: a new atmospheric probe," *Quart. J. Roy. Meteorol. Soc.* **92,** 220-230 (1966).

5. Klett., J.D., "Stable analytical inversion solution for processing LIDAR returns," *Appl. Opt.* **20**, 211-220 (1981).

6. Fernald, F.G., "Analysis of atmospheric LIDAR observations: Some comments," *Appl. Oppt*. **23**, 652-653 (1984).

7. Noxon, J. F., "Nitrogen dioxide in the stratosphere and troposphere measured by ground-based absorption spectroscopy," *Science* **189**, 547 (1975).

8. Noxon, J. F., E. C. Whipple, and R. S. Hyde, "Stratospheric NO_2. 1. Observational method and behaviour at midlatitudes," *J. Geophys. Res.* **84**, 5047-5076 (1979).

9. Solomon, S., A. L. Schmeltekopf, and R. W. Sanders, "On the interpretation of zenith-sky absorption measurements," *J. Geophys. Res.* **92**, 8311-8319 (1987).

10. Otten, C., F. Ferlemann, U. Platt, T. Wagner, and K. Pfeilsticker, "Groundbased DOAS UV/visible measurements at Kiruna (Sweden) during the SESAME winters 1993/94 and 1994/95," *J. Atm. Chem.* **30**, 141-162 (1998).

11. Aliwell, S.R., P.V. Johnston, A. Richter, M. Van Roozendael, T. Wagner, D.W. Arlander, J.P. Burrows, D.J. Fish, R.L. Jones, K. Karlsen Tørnkvist, J.-C. Lambert, K. Pfeilsticker and I. Pundt, "Analysis for BrO in zenith-sky spectra - an intercomparison exercise for analysis improvement," *J. Geophys. Res*. **107**, 10.1029/2001JD000329 (2002).

12. Perner, D. and U. Platt, "Detection of nitrous acid in the atmosphere by differential optical absorption," *Geophys. Res. Lett*. **7**, 1053-1056 (1979).

13. Platt, U., D. Perner, and W. Pätz, "Simultaneous measurements of atmospheric CH_2O, O_3 and NO_2 by differential optical absorption," *J. Geophys. Res,* **84**, 6329-6335 (1979).

14. Platt, U., "Differential optical absorption spectroscopy (DOAS), in Air Monitoring by Spectroscopic Techniques," *M. W. Sigrist (Ed.), Chemical Analysis Series* **127** (J. Wiley, New York, 1994).

15. Hönninger G., and Platt U., "The Role of BrO and its Vertical Distribution during Surface Ozone Depletion at Alert," *Atmos. Environ*. **36**, 2481–2489 (2002).

16. Leser, H., Hönninger, G., and Platt, U., "MAX-DOAS measurements of BrO and NO2 in the marine boundary layer," *Geophys. Res. Lett.* **30**, doi:10.1029/2002GL015811, (2003).

17. Von Friedeburg, C., I. Pundt, K.-U. Mettendorf, T. Wagner, and U. Platt, "Multi-AXis-(MAX) DOAS Measurements of NO_2 during the BAB II Motorway Emission Campaign," *Atmospheric Environment* **39**, 977-985 (2003).

18. Bobrowski, N., Hönninger, G., Galle, B., and Platt, U., "Detection of bromine monoxide in a volcanic plume," *Nature* **423**, 273–276 (2003).

19. Van Roozendael, M., Fayt, C., Post, P., Hermans, C., Lambert, J.-C., "Retrieval of BrO and NO_2 from UV-Visible Observations," in: *Sounding the troposphere from space: a new era for atmospheric chemistry, Springer-Verlag, ISBN 3-540-40873-8, edited by Borell, P. et al.,* 155-165, (2003).

20. Wittrock, F., H. Oetjen, A. Richter, S. Fietkau, T. Medeke, A. Rozanov, and J. P. Burrows, "MAX-DOAS measurements of atmospheric trace gases in Ny-Ålesund," *Atmos. Chem. Phys.* **4**, 955-966 (2004).

21. Hönninger, G., C. von Friedeburg, and U. Platt, "Multi Axis Differential Optical Absorption Spectroscopy (MAX-DOAS)," *Atmos. Chem. Phys*. **4**, 231-254 (2004).

22. Heckel, A., A. Richter, T. Tarsu, F. Wittrock, C. Hak, W. Junkermann, and J. Burrows, "DOAS off-axis measurements of Formaldehyde," *Atmos. Chem. Phys.* **5**, 909–918 (2005).

23. Wagner, T., B. Dix, C.v. Friedeburg, U. Frieß, S. Sanghavi, R. Sinreich, and U. Platt, "MAX-DOAS O_4 measurements – a new technique to derive information on atmospheric aerosols. (I) Principles and information content," *J. Geophys. Res.* **109**, doi:10.1029/2004JD004904, (2004).

24. Sinreich, R., U. Frieß, T. Wagner, and U. Platt, "Multi axis differential optical absorption spectroscopy (MAX-DOAS) of gas and aerosol distributions," *Faraday Discuss*. **130**, doi:10.1039/b419274p, (2005).

25. Marquard, L.C., T. Wagner, and U. Platt, Improved Air Mass Factor Concepts for Scattered "Radiation Differential Optical Absorption Spectroscopy of Atmospheric Species," *J. Geophys. Res.* **105**, 1315-1327 (2000).

26. Galle, B., "30 Month Management Report-DORSIVA, Development of Optical Remote Sensing Instruments for Volcanological Applications - Reporting period: 1 October 2004 - 31 March 2005," EC contract: EVG1 (CT2002-00060), (2005).

27. Hartl, A., Song, B.C. and Pundt, I., "2D Reconstruction of Atmospheric Concentration Peaks from Long-Path DOAS Measurements: Parametrisation and Geometry within a Discrete Approach," submitted for publication to *Atmos. Chem. Phys*., (2005).

28. Stutz, J. and U. Platt, "Numerical Analyses and Estimation of the Statistical Error of Differential Optical Absorption Spectroscopy Measurements with Least Square Methods," *Appl. Opt.* **35**, 6041-6053 (1996).

29. Wagner, T., C. von Friedeburg, M. Wenig, C. Otten, and U. Platt, "UV/vis observations of atmospheric O_4 absorptions using direct moon light and zenith-scattered sunlight under clear and cloudy sky conditions," *J. Geophys. Res.* **107**(20), 4424, doi:10.1029/2001JD001026, (2002).

30. Erle F., K. Pfeilsticker, and U. Platt, "On the influence of tropospheric clouds on zenith-scattered-light measurements of stratospheric species," *Geophys. Res. Lett.* **22**, 2725- 2728 (1995).

31. Veitel V., O. Funk, C. Kurz, U. Platt, and K. Pfeilsticker, "Geometrical path length probability density function of the skylight transmitted by mid-latitude cloudy skies; Some case studies," *Geophys. Res. Lett.* **25**, 3355-3358 (1998).

32. Wagner, T., F. Erle, L. Marquard, C. Otten, K. Pfeilsticker, T. Senne, J. Stutz, and U. Platt, "Cloudy sky optical paths as derived from differential optical absorption spectroscopy observations," *J. Geophys. Res.* **103**, 25307-25321 (1998).

33. Galle, B., Oppenheimer, C., Geyer, A., McGonigle, A., Edmonds, M. & Horrocks, L., "A miniaturised ultraviolet spectrometer for remote sensing of SO_2 fluxes: a new tool for volcano surveillance," *J. of Volc. and Geotherm. Res*. **119**, 214-254 (2003).

34. Rodgers, C., "Retrieval of atmospheric temperature and composition from remote measurements of thermal radiation," *Rev. Geophys. Space Phys.* **14**, 609–624 (1976).

35. Rodgers, C. D., *Inverse Methods for Atmospheric Sounding*, World Scientific, London, (2000).

36. Bobrowski, N. and U. Platt, "Bromine Monoxide Studies in Volcanic Plume". *J. of Volc. and Geotherm. Res.,* (2005), submitted for publication.

37. Bussemer, M. „Der Ring-effekt: Ursachen und Einfluss auf die spektroskopische Messung stratosphaerischer Spurenstoffe" *Diploma thesis, Institut fuer Umweltphysik, Universitaet Heidelberg,* (1993).

38. Fayt, C. and M. van Roozendael, WinDOAS 2.1—Software User Manual Belgisch Instituut voor Ruimte-Aeronomie Institut d'Aéronomie Spatiale de Belgique, Brussels, Belgium, (2001).

39. Bogumil, K., J. Orphal, T. Homan, S. Voigt, P. Spietz, O. Fleischmann, A. Vogel, M. Hartmann, H. Bovensmann, J. Frerick, and J. Burrows. „Measurements of molecular

absorption spectra with the SCIAMACHY Pre-Flight Model: instrument characterization and reference data for atmospheric remote-sensing in the 230-2380 nm region". *Journal of Photochemistry and Photobiology A: Chemistry,* Vol. 157, 167-184, (2003).

40. Voigt, S., J. Orphal, and J. P. Burrows. "UV-visible absorption cross-sections of NO_2 and O_3 at atmospheric temperatures and pressures by FTS". In *Proc. of the 1st Europ. Symp. Atmos. Meas. from Space* (ESAMS-99), ESA-ESTEC, Noordwijk, The Netherlands, ESA WPP-161, Vol. 2, 443-465 (1999).

41. Hermans, C., A. C. Vandaele, M. Carleer, S. Fally, R. Colin, A. Jenouvrier, B. Coquart, and M.-F.M¶erienne. Absorption Cross-Sections of Atmospheric Constituents: NO2, O2, and H2O. *Environ. Sci. & Pollut. Res.,* Vol. 6, No. 3, 151-158, (1999).

42. Vandaele, A. C., C. Hermans, P. C. Simon, M. Carleer, R. Colin, S. Fally, M.-F. Mérienne, A. Jenouvrier, and B. Coquart, "Measurements of the NO_2 Absorption Cross-section from 42000 cm^{-1} to 10000 cm^{-1} (238-1000 nm) at 220 K and 294 K," *J. Quant. Spectrosc. Radiat. Transfer* **59**, 171-184 (1997).

43. Vandaele, A.C., C. Fayt, F. Hendrick, C. Hermans, F. Humbled, M. Van Roozendael, M. Gil, M. Navarro, O. Puentedura, M. Yela, G. Braathen, K. Stebel, K. Tørnkvist, P. Johnston, K. Kreher, F. Goutail, A. Mieville, J.-P. Pommereau, S. Khaikine, A. Richter, H. Oetjen, F. Wittrock, S. Bugarski, U. Frieß, K. Pfeilsticker, R. Sinreich, T. Wagner, G. Corlett, and R. Leigh, "An intercomparison campaign of ground-based UV-visible measurements of NO_2, BrO, and OClO slant columns: Methods of analysis and results for NO2," *J. Geophys. Res.*, **110**, doi:10.1029/2004JD005423, (2005).

44. Greenblatt G. D., J.J. Orlando, J.B. Burkholder, and A.R. Ravishankara, Absorption measurements of oxygen between 330 and 1140 nm, *J. Geophys. Res., 95,* 18577-18582 (1990).

45. Buchwitz, M., R. de Beek, K. Bramstedt, S. Noël, H. Bovensmann, and J. P. Burrows, "Global carbon monoxide as retrieved from SCIAMACHY by WFM-DOS," *Atmos. Chem. Phys.* **4**, 1954-1960 (2004).

46. Frankenberg, C., J.F. Meirink, M. van Weele, U. Platt, and T. Wagner, "Assessing methane emissions from global space-borne observations," *Science* **308** (5724):1010-1014, (2005).

47. Frankenberg, C., U. Platt, T. Wagner, "Retrieval of CO from SCIAMACHY onboard ENVISAT: detection of strongly polluted areas and seasonal patterns in global CO abundances," *Atmos. Chem. Phys*. **5**, 1639-1644 (2005).

FIGURE CAPTIONS

Fig. 1. – Experimental set-up for tomographic MAX-DOAS observations. In contrast to conventional MAX-DOAS observations the telescope is directed towards targets, which are illuminated by the sun. The total signal contains the trace gas absorptions of two sections of the total light path: between the targets and the top of the atmosphere (paths A_1, A_2, A_3) and between the instrument and the targets (paths B, C, D). After correction for the absorption from the section between the targets and the top of the atmosphere (see Section 2.B.) the average trace gas concentration between the instrument and the target can be analyzed. If several targets are used, even more-dimensional trace gas distributions can be retrieved.

Fig. 2. – Composition of the light received by the telescope: Sunlight can be reflected by the target or scattered by molecules and aerosols between the target and the instrument.

Fig. 3. – Dependence of the measured radiance (top) and the sensitivity *R* (bottom) as a function of the distance from the instrument for different measurement conditions. For an optically thin atmosphere and a bright target (case 1) most of the received light originates from the target and the sensitivity does not depend on the distance from the instrument. For an optically thin atmosphere and a black target (case 2) the light originates only from atmospheric scattering and the received radiance is constant over the line of sight. The sensitivity decreases linearly with distance from the instrument. For an optically thick atmosphere (case 3) all light from distant paths is almost completely extinguished and the scattered light originates only from air masses close to the instrument. The sensitivity of the measurement is restricted only to air masses very close to the instrument.

Fig. 4 – Possible two-dimensional tomographic set-up using two instruments and three targets. The different lines of sight ('rays') cross different boxes of the discretized concentration field. Ray AA is sensitive to the trace gas concentration in boxes 11, 21, and 31; ray BB is sensitive to the concentrations in boxes 21 and 22, etc. Please note that additional rays between instrument A and targets B and C are possible.

Fig. 5 – Viewing directions of the telescope: The hills behind the left viewing direction (short path, sp) are about 1.9 km distant. The hills behind the right viewing direction (long path, lp) is about 3.3 km distant and the path crosses the old part of Heidelberg (see Fig. 6)

Fig. 6 – Map of Heidelberg with the horizontal light paths between the instrument and the hills.

Fig. 7 – Spectral analysis of the measured NO_2 absorption for a measurement in the afternoon (temporal resolution about 3 min). One measurement from the longer light path is analyzed using a zenith spectrum (at 15: 06) as Fraunhofer spectrum. The same spectra analyzed using a shorter light path (taken at 15:26) as Fraunhofer spectrum is displayed in the lower panel. In the spectral analysis the cross section of NO_2 (for 294 K)[42], a Ring spectrum and a second order polynomial were included.[11]

Fig. 8 – Comparison of the resulting NO_2 SCDs using the zenith-sky observations (taken at 15:06) as reference (left) or using the spectra of the short light path as reference (taken at 15:27) for the spectra of the long light path (right). The latter are almost the same as the difference between the results for both directions. Only the one sigma fitting errors are accounted for the error bars. The measurement sequence is described in the text.

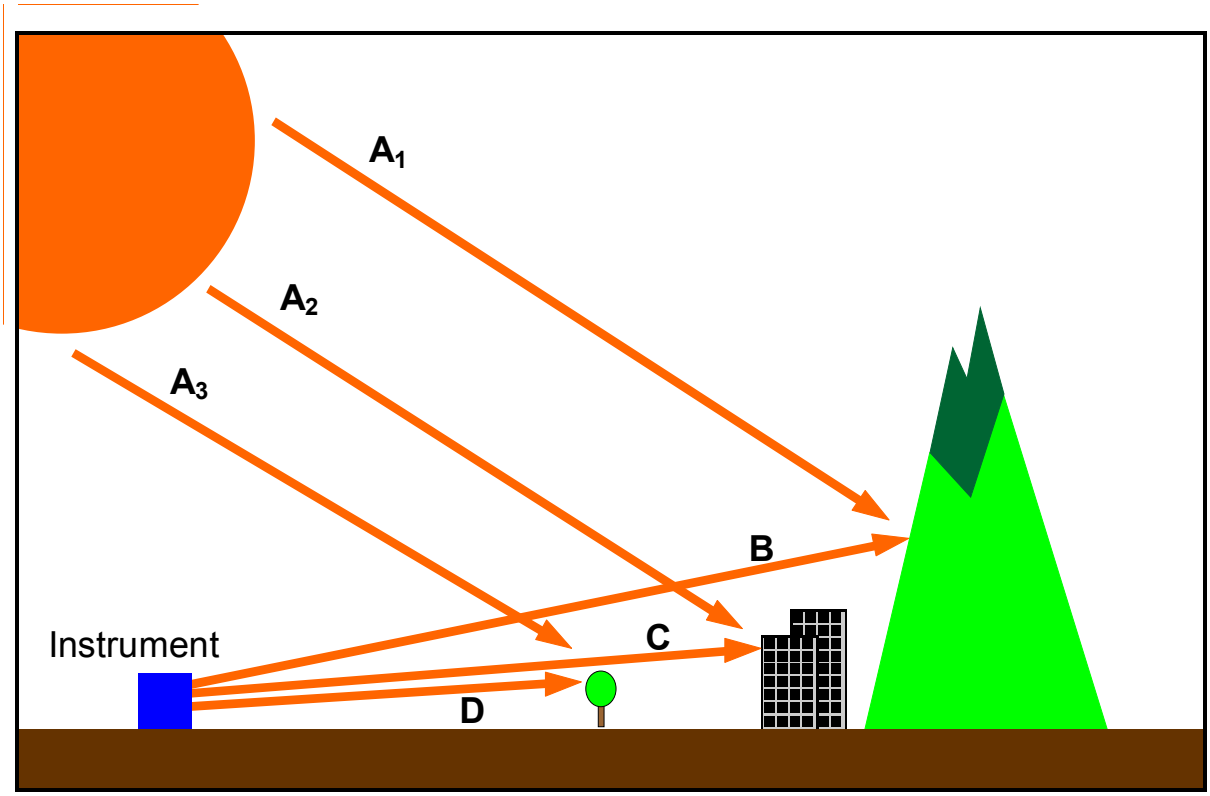

FIGURE 1

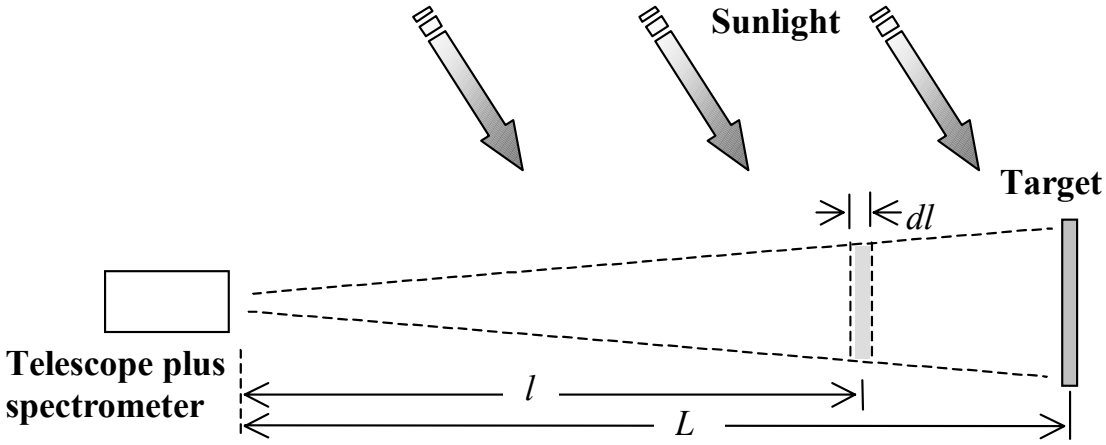

FIGURE 2

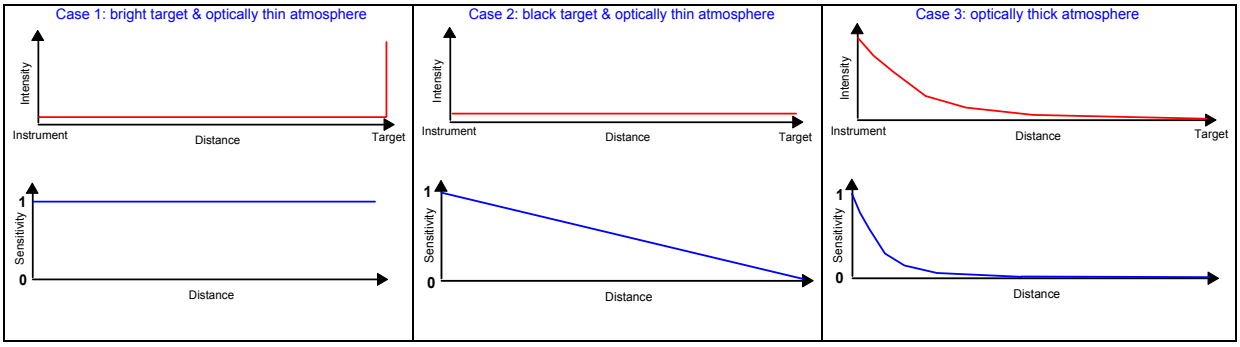
Case 1: bright target & optically thin atmosphere
Intensity
Instrument
Distance
Target
Sensitivity
1
0
Distance
Case 2: black target & optically thin atmosphere
Intensity
Instrument
Distance
Target
Sensitivity
1
0
Distance
Case 3: optically thick atmosphere
Intensity
Instrument
Distance
Target
Sensitivity
1
0
Distance

FIGURE 3

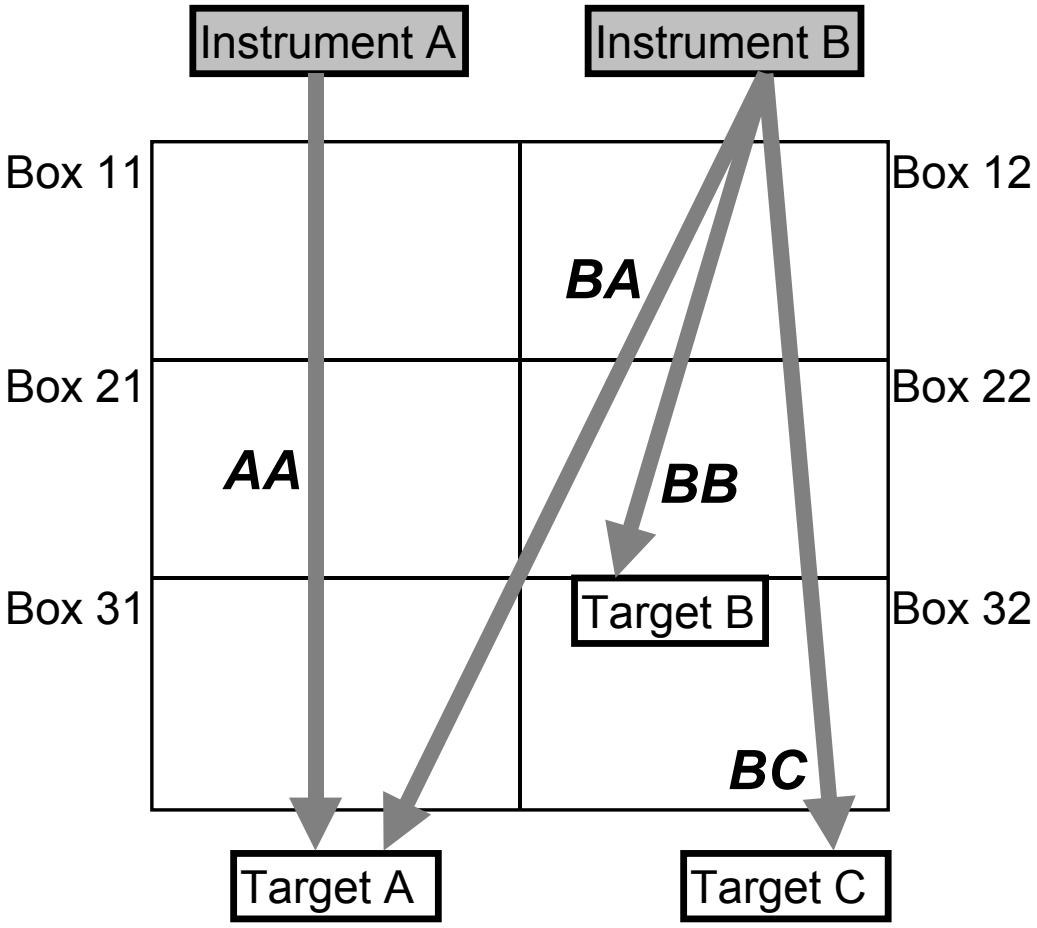
Instrument A
Instrument B
Box 11
Box 12
BA
Box 21
Box 22
AA
BB
Box 31
Target B
Box 32
BC
Target A
Target C

FIGURE 4

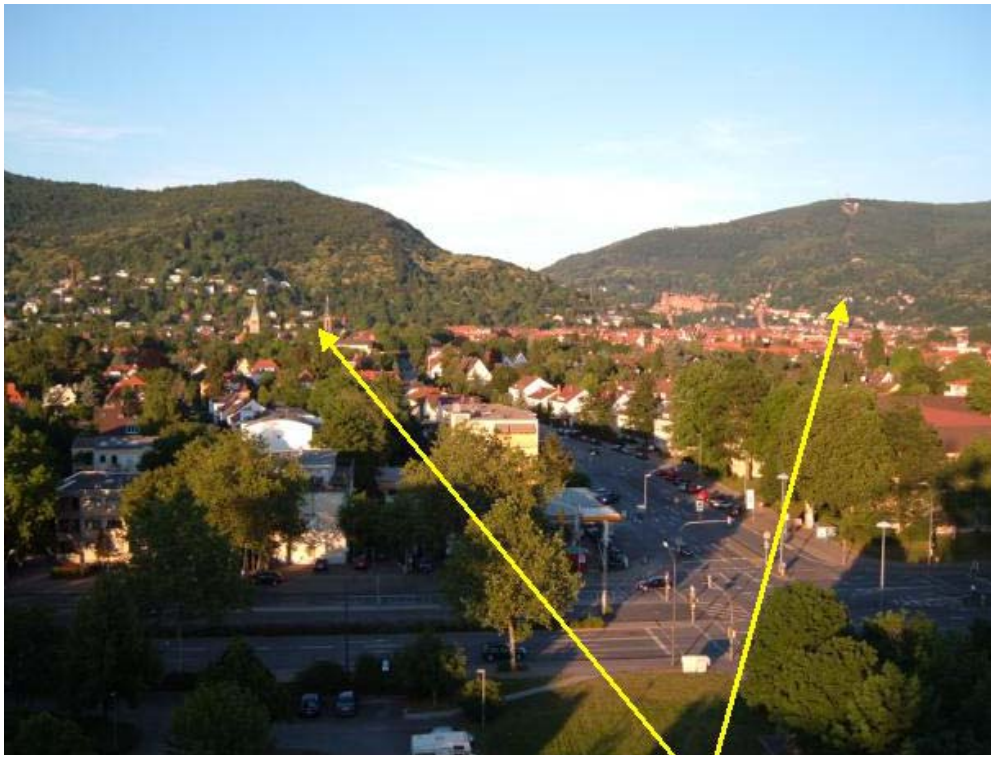

FIGURE 5

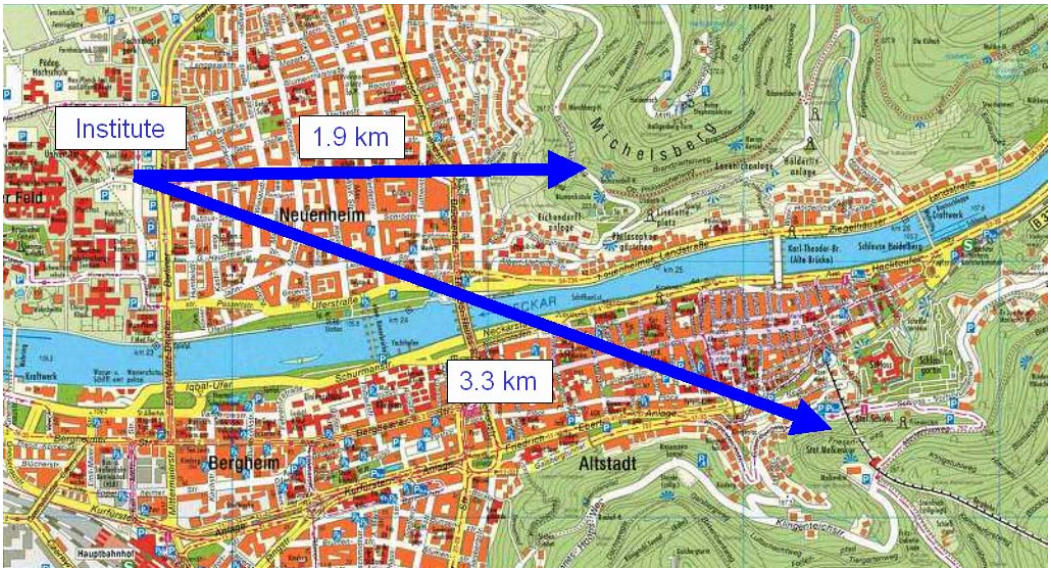
Institute
1.9 km
3.3 km
Neuenheim
Bergheim
Altstadt
Michelsberg

FIGURE 6

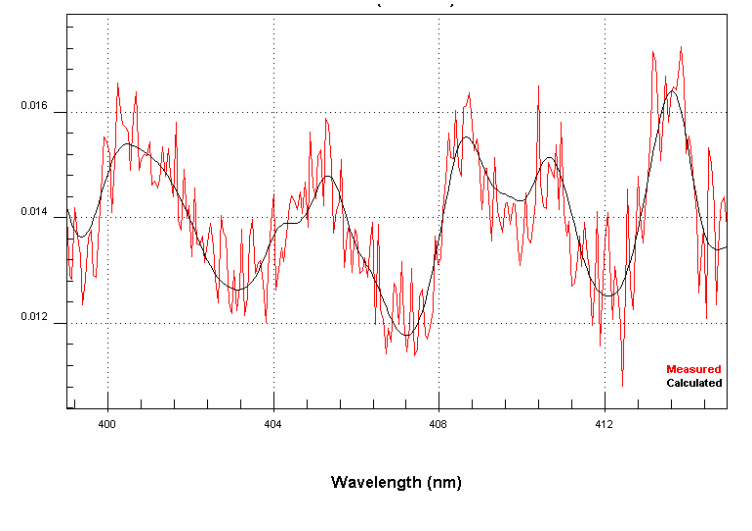
0.016
0.014
0.012
400
404
408
412
Measured
Calculated
Wavelength (nm)

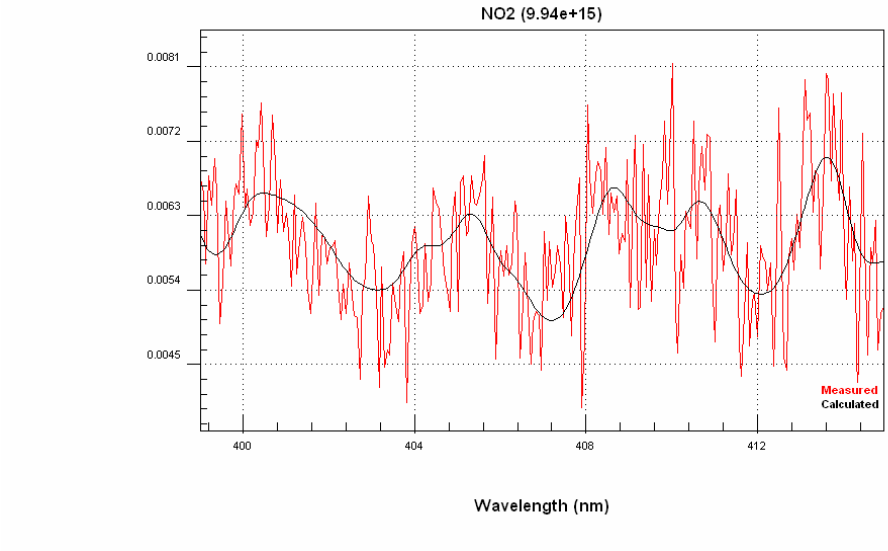
NO2 (9.94e+15)
0.0081
0.0072
0.0063
0.0054
0.0045
400
404
408
412
Measured
Calculated
Wavelength (nm)

FIGURE 7

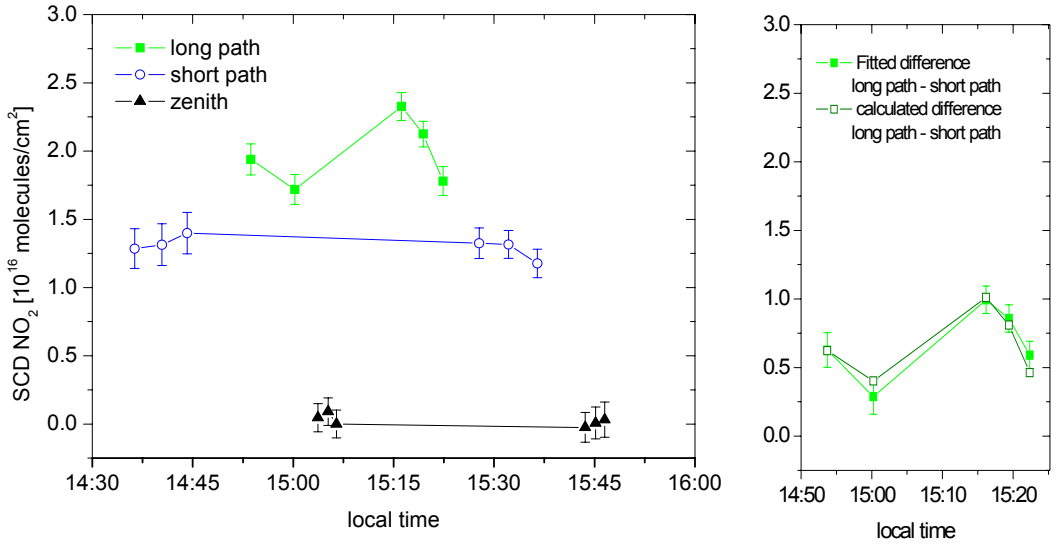
long path
short path
zenith
SCD NO2 [10^16 molecules/cm^2]
local time
Fitted difference
long path - short path
calculated difference
long path - short path
local time

FIGURE 8

TABLE CAPTION

Table 1. To derive the SCDs of NO_2 and O_4 the spectra were analyzed using the Software WinDOAS V2.10 from IASB (Belgium Institute for Space Aeronomy [38], which applies a nonlinear least squares method.[28] The Ring spectrum was calculated from the measured zenith sky spectrum (taken at 15: 06) by using the DOASIS software.[37]

Table 2. Measured and true SCDs as well as average concentrations and mixing ratios of NO_2 for the measurement taken at 15:16 (see Fig. 7). (For the evaluation were used the short light path reference spectrum at 15:26 and the zenith sky spectrum taken at 15:06.)

Analysed Trace gas	**Used cross section**	**polynomial**	**Spectral range**
NO_2	NO_2(294K)[40]	2nd order	399 - 415 nm
O_4	NO_2(294K)[40], O_4[41], O_3(223K)[39], O_3(246K)[39]	3rd order	352 – 387 nm

TABLE 1

Path	**Analysed NO_2 SCD (S_{meas})**	**True NO_2 SCD (S_{target})**	**Path length**	**Average NO_2 concentration**	**Average NO_2 mixing ratio**
Long path - short path	1.0×10^{16} molec/cm²	1.25×10^{16} molec/cm²	1.9 km	6.6×10^{10} molec/cm³	2.5 ppb
long path	2.3×10^{16} molec/cm²	3.15×10^{16} molec/cm²	3.3 km	9.6×10^{10} molec/cm³	3.7 ppb

TABLE 2